Supplementary Figures

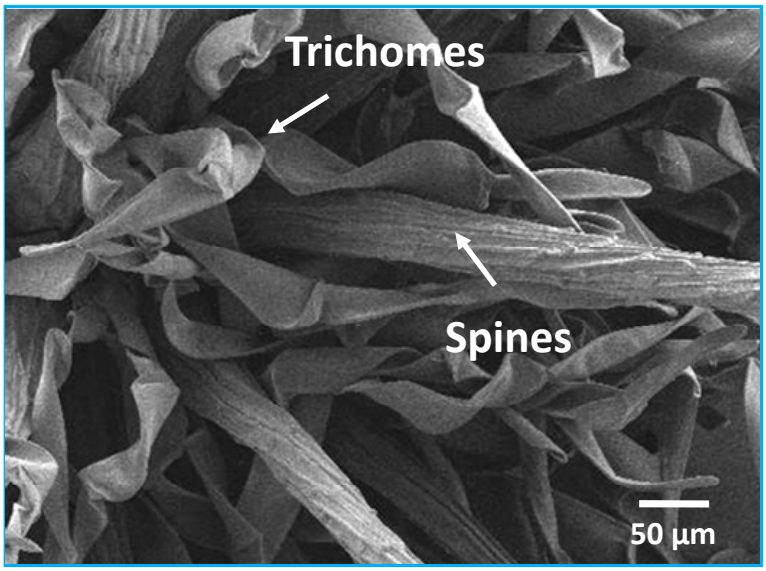

Supplementary Figure S1 | The structure of the trichomes at the base of cactus spines. These trichomes have a width of approximately 28.6 µm, a thickness of approximately 3.4 µm, and a length of approximately 606.9 µm.

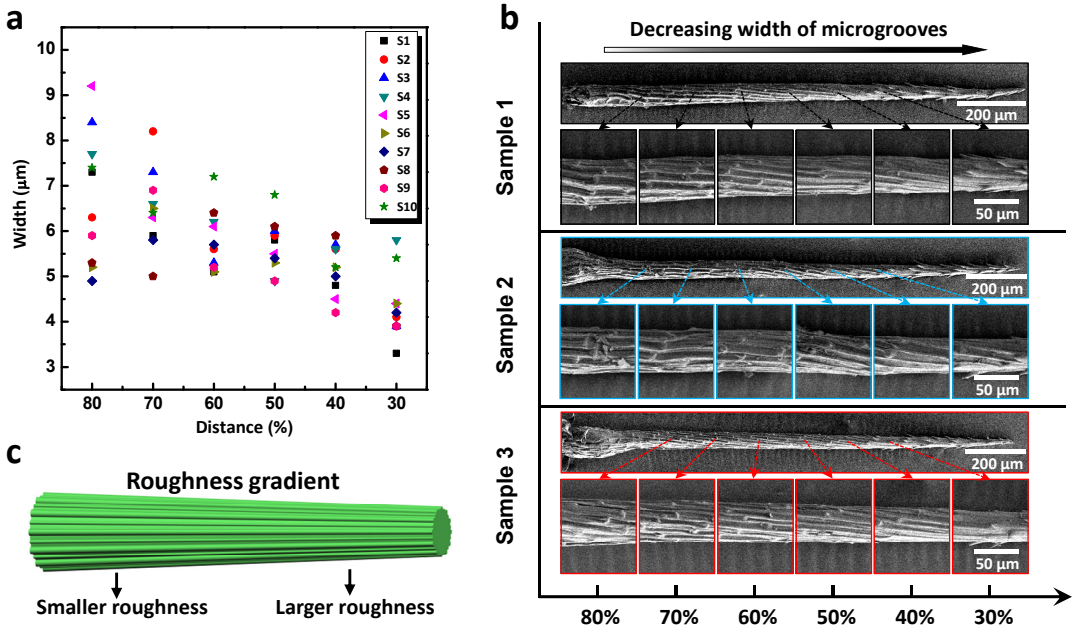

Supplementary Figure S2 | Statistical measurements of the gradient microgrooves along the cactus spines. **a,** Ten cactus spines were selected randomly; for each spine, the average widths of the microgrooves at 80%, 70%, 60%, 50%, 40% and 30% of the entire spine length away from the tip were measured. From the region near the base to the location near the tip (80% to 30%), the width of these microgrooves decreased. **b,** Three representative cactus spine SEM images (Sample 1, Sample 2 and Sample 3) illustrate the width gradient of the microgrooves along the cactus spines. For each spine, the lower six images correspond with the six regions (80%, 70%, 60%, 50%, 40% and 30% of the entire spine length away from the tip) on the upper single spine. The microgrooves near the base are wider than those near the tip. **c,** The gradient of the microgrooves in the middle of the spine gives rise to a gradient of roughness along the spine; the roughness near the base is smaller than at the top.

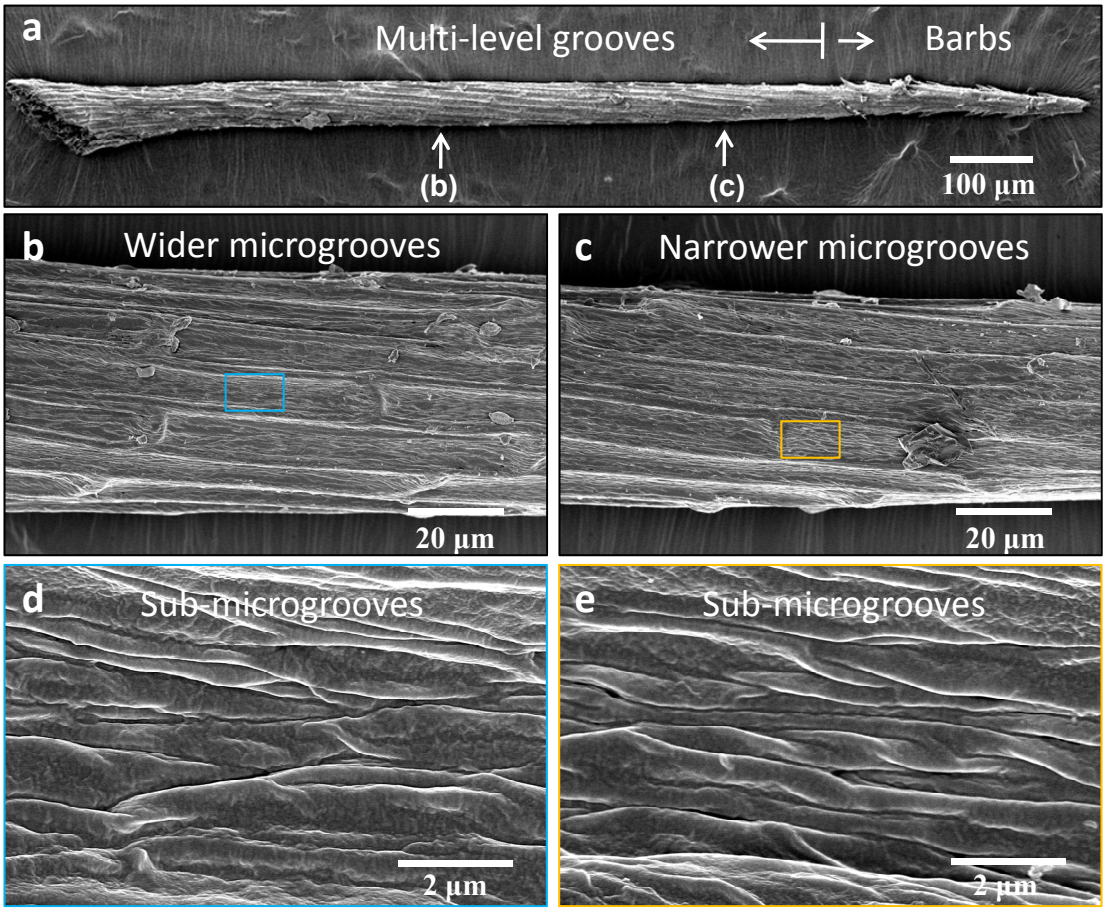

Supplementary Figure S3 | Detailed observations of the multi-level grooves along the cactus spines. **a,** SEM image of a spine. The tip was covered with oriented barbs, while the middle was covered with multi-level grooves and was divided into two regions **(b)** and **(c)** with different grooved structures. **b-c,** Magnified images of regions **(b)** and **(c)**. The width of the microgrooves on the cactus spine near the base was larger than the width near the tip. **d-e,** Magnified images of the areas depicted with the blue and yellow boxes in **b** and **c,** respectively. The sub-micron grooves near the base and tip demonstrated no significant differences.

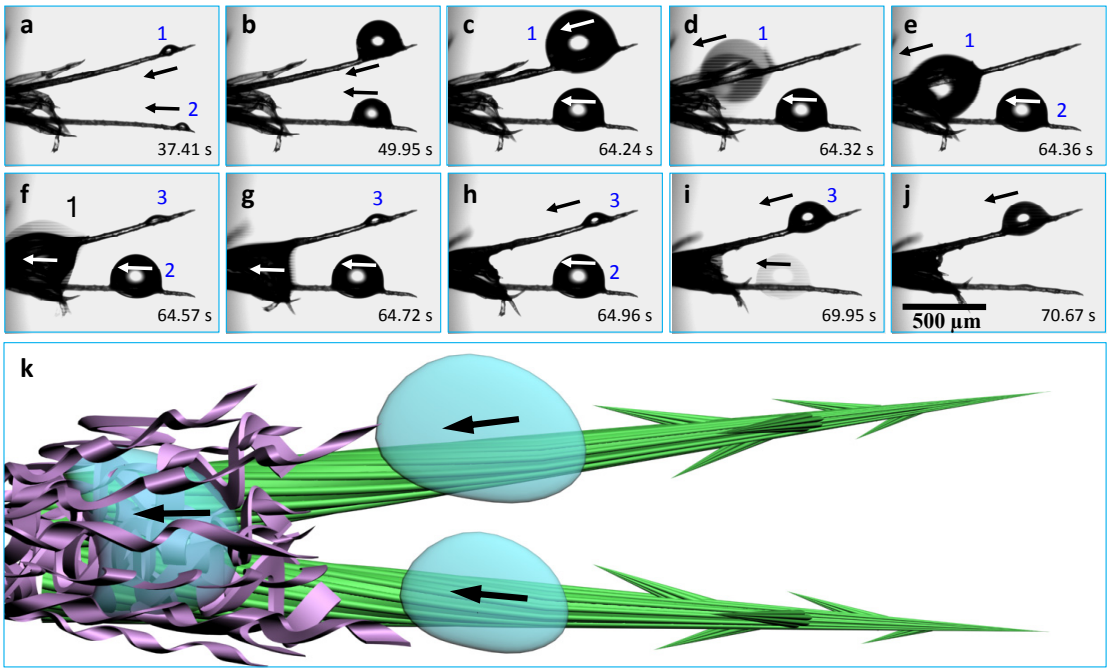

Supplementary Figure S4 | *In situ* optical microscopic observation and an illustration of the absorption process of the water drops on two adjacent spines with clustered trichomes at the base. **a,** Two water drops denoted as 1 and 2 were collected on the two adjacent spines and moved toward the base of the spines with increasing size (**b-c**). **d-g,** As water drop 1 contacted the trichomes, an immediate absorption occurred within a half second (from 64.32 s to 64.72 s). A new collection cycle began with the appearance of drop 3. **h-j,** Water drop 2 also moved along the spine to be absorbed by the same trichomes. **k,** The scheme illustrates the behaviour of the water drops on adjacent spines. These water drops were quickly absorbed upon contact with the trichomes.

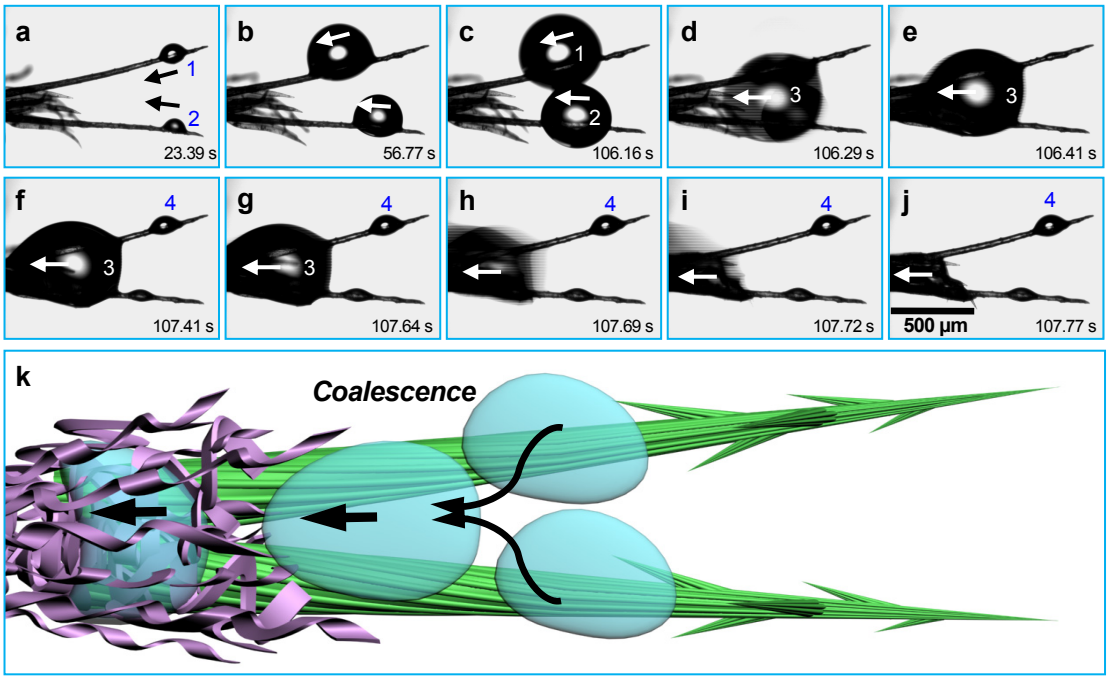

Supplementary Figure S5 | *In situ* optical microscopic observation and an illustration of the coalescence and the absorption process of the water drops on two adjacent spines with clustered trichomes at the base. **a,** Two water drops (denoted as 1 and 2) were collected on two adjacent spines and transported toward the base of the spines with increasing size (**b**). **c-d,** Water drops 1 and 2 were located close enough to coalesce into larger drop 3. **e-j,** The coalesced water drop 3 was quickly absorbed upon contact with the trichomes. A new collection cycle began with the appearance of drop 4. **k,** The scheme illustrates the movement behaviour of the water drops on adjacent spines. These water drops coalesced to form larger drops that were subsequently absorbed upon contact with the trichomes.

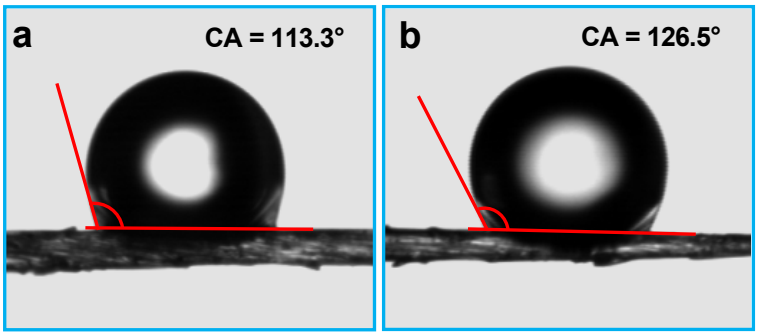

Supplementary Figure S6 | Typical optical images of two sessile water drops on the regions near the base and the tip of a cactus spine. The water contact angle near the base (**a**) and the tip (**b**) is approximately 113.3° and 126.5°, respectively.

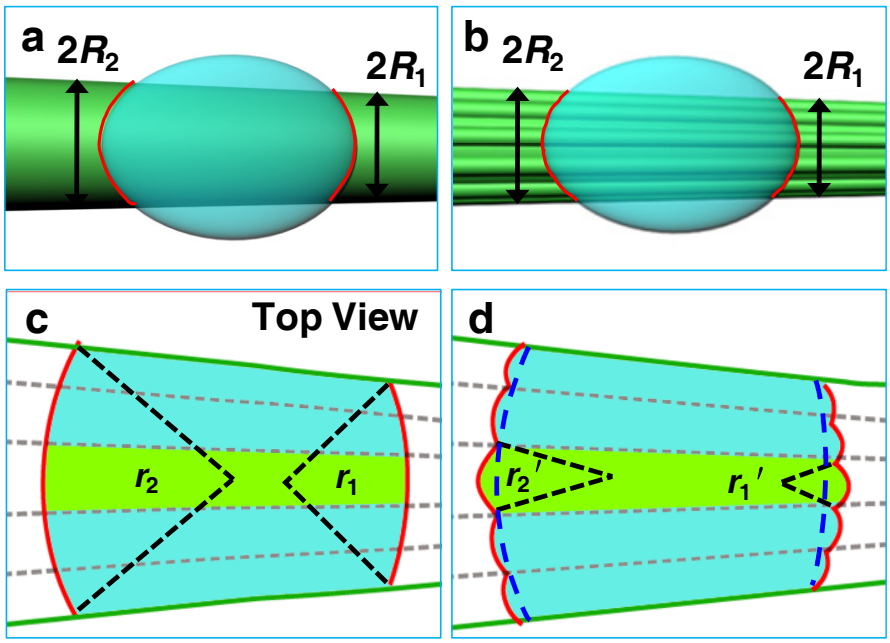

Supplementary Figure S7 | Comparison of the gradient of the Laplace pressure along the smooth and the grooved conical spines. Water drop sites on the conical spine with a smooth surface **(a)** and gradient grooves **(b)**. The circular-arc-shaped red lines denote the corresponding three-phase contact lines (TCLs). $2R_1$ and $2R_2$ are the local diameters of the spines. **c-d,** Top-view images of the liquid-solid contact area. The blue dashed lines in **(d)** correspond with the red lines in **(c)**. The local curvature radii r_1 (r_2) and r_1' (r_2') of the TCLs on the smooth surface and the gradient grooved surface with $r_1' < r_1$, $r_2' < r_2$. Assuming the very small liquid-solid contact area to be a flat surface, as shown by the green colour in the 'Top View' images, the Laplace pressure difference of this small area on a gradient grooved surface $\gamma(\frac{1}{r_1'}-\frac{1}{r_2'})$ is larger than that on a smooth surface $\gamma(\frac{1}{r_1}-\frac{1}{r_2})$.

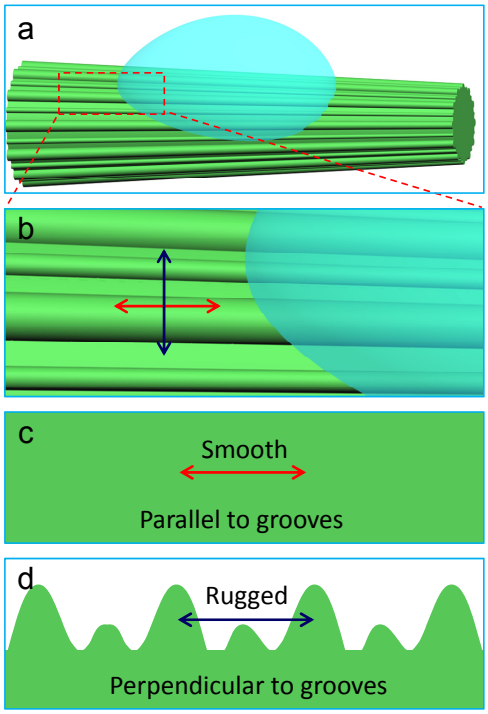

Supplementary Figure S8 | Anisotropic hysteresis of the water drops moving on the grooved cactus spines. **a,** A water drop moving on the grooved cactus spine. **b,** Magnified region near TCL indicated in **(a)** by a red rectangle. The red and blue arrows denote the motion parallel and perpendicular to the grooves, respectively. **c-d,** the motion parallel to the grooves had a relatively small hysteresis that was identical to that on a smooth surface **(c).** The motion perpendicular to the grooves had an increased hysteresis that was identical to that observed for a rugged surface **(d)**.

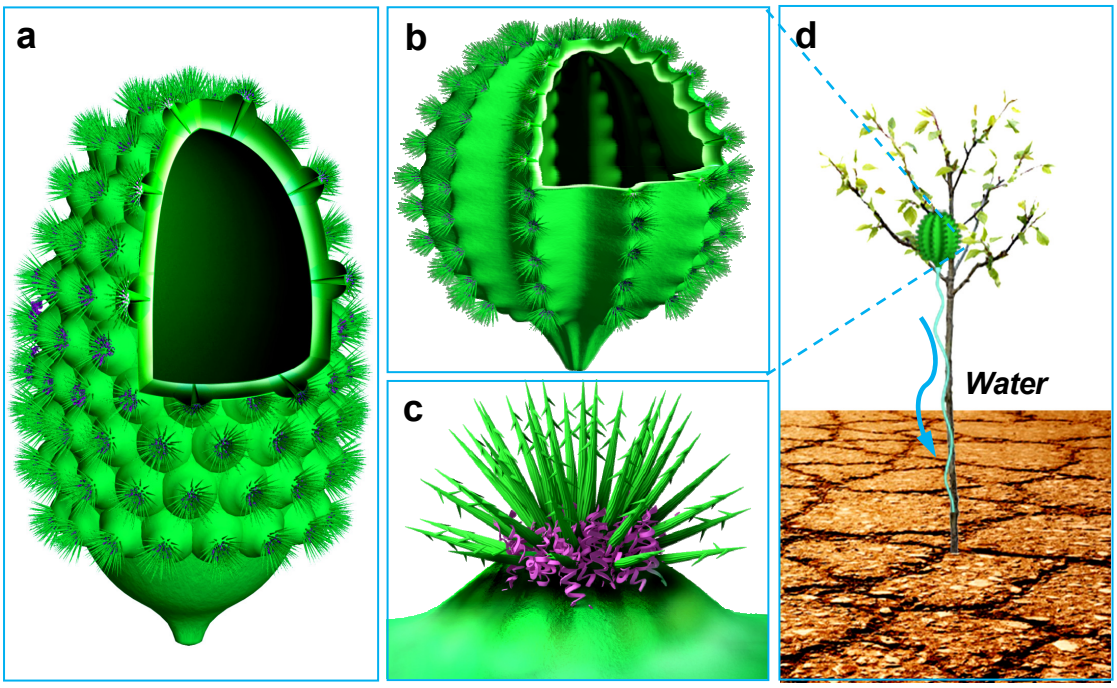

Supplementary Figure S9 | Schematic diagrams of the application of a bio-mimicking artificial continuous fog collection system with different outer contours and surface structures. **a-b**, Two types of artificial fog collection systems. Clustered conical spines dispersed evenly on the ellipsoid with the hemispherical structures covered **(a)** and on the sphere with the ridges covered **(b)**. **c,** Magnified single cluster of spines with conical barbs on the tip side, gradient grooves on the middle side, and belt-structured trichomes on the base side. **d,** A sapling living in the arid environment can obtain water supply from the artificial fog collection system suspended from the sapling.

Supplementary Note 1

Background and design principles of the artificial fog collector. Fog has been widely recognised as an important alternative water source in many regions worldwide. Bio-inspired artificial fog collectors have been extensively studied, and many products, such as the two-dimensional planar collector[36], the standard fog collector[37] and the three-dimensional omnidirectional fog collector[38], have been developed.

Water drops collected on these collectors rely primarily on the force of gravity to convey the water to the containers attached below. The openings of the water containers designed for catching the water drops may also increase the risk of evaporation. Inspired by the integral fog collection system of the cactus *O. microdasys*, we designed a three-dimensional, omnidirectional fog collector by introducing the main characteristics of the cactus without considering the boundary layer problems. The fog collector based on this basic idea could collect water drops from fog, directing the water to a container without the use of gravitational force or wind velocity. In addition, the water container embedded in the collector did not require a large opening, decreasing evaporation.

A consideration of the boundary layer[40-41] on the surface of the artificial fog collector indicated that a smaller size of the construction would have been a better choice.

Supplementary References

40 Martorell, C. & Ezcurra, E. The narrow-leaf syndrome: a functional and evolutionary approach to the form of fog-harvesting rosette plants. *Oeologia* **151**, 561-573 (2007).

41 Ritter, A. & Regalado, C. M. Fog water collection in a subtropical Elfin Laurel Forest of the Garajonay National Park (Canary Islands): a combined approach using artificial fog catchers and a physically based impaction model. *J. Hydrometeorol.* **9**, 920-935 (2008).